Atmos. Chem. Phys. Discuss., 12, 7793–7827, 2012
www.atmos-chem-phys-discuss.net/12/7793/2012/
doi:10.5194/acpd-12-7793-2012

Atmospheric Chemistry and Physics Discussions

A stratospheric intrusion at the subtropical jet over the Mediterranean Sea: air-borne remote sensing observations and model results

K. Weigel[1,*], **L. Hoffmann**[1,**], **G. Günther**[1], **F. Khosrawi**[2], **F. Olschewski**[3], **P. Preusse**[1], **R. Spang**[1], **F. Stroh**[1], **and M. Riese**[1,3]

[1]Institute of Energy and Climate Research (IEK-7), Forschungszentrum Jülich, 52425 Jülich, Germany
[2]Department of Meteorology, Stockholm University, 10691 Stockholm, Sweden
[3]Department of Physics, University of Wuppertal, 42907 Wuppertal, Germany
[*]now at: Institute of Environmental Physics (IUP), University of Bremen, 28359 Bremen, Germany
[**]now at: Juelich Supercomputing Centre (JSC), Forschungszentrum Jülich, 52425 Jülich, Germany

Received: 2 February 2012 – Accepted: 9 March 2012 – Published: 20 March 2012

Correspondence to: K. Weigel (weigel@iup.physik.uni-bremen.de)

Published by Copernicus Publications on behalf of the European Geosciences Union.

Abstract

Remote sensing measurements from the Cryogenic Infrared Spectrometers and Telescope for the Atmosphere – New Frontiers (CRISTA-NF) during a flight on 29 July 2006 are presented. This flight is part of the AMMA-SCOUT-O3 measurement campaign, where CRISTA-NF was deployed on the high-flying research aircraft M55-Geophysica. The flight path was located over Italy and the Mediterranean Sea and crossed over the subtropical jet twice. Measurements of temperature, and the volume mixing ratios of water vapor (H_2O), ozone (O_3), nitric acid (HNO_3) and peroxyacetyl nitrate (PAN) are available with a vertical resolution of up to 500 m between about 6 to 21 km altitude. CRISTA-NF observes these trace gases simultaneously and provides a quasi-2D view of the transition region between the troposphere and the stratosphere. The observation of these different trace gases allows to determine the origin of air masses in the stratosphere or troposphere. As expected, higher abundances are found where the main source of the trace gases is located: in the stratosphere for O_3 and in the troposphere for H_2O and PAN. Tracer-tracer correlations between O_3 and PAN are used to identify mixed tropospheric and lowermost stratospheric air at the subtropical jet and around the thermal tropopause north of the jet. An intrusion of stratospheric air into the troposphere associated with the subtropical jet is found in the CRISTA-NF observations. The observations indicate that the intrusion is connected to a tropopause fold which is not resolved in the ECMWF analysis data. The intrusion was reproduced in a simulation with the Chemical Lagrangian Model of the Stratosphere (CLaMS). This work discusses the nature of the observed processes at the subtropical jet based on the CRISTA-NF observations and the CLaMS simulation.

1 Introduction

The Upper Troposphere, Lower Stratosphere (UTLS) is an atmospheric layer where strong gradients of e.g. trace gases and wind speeds exist both vertically and horizon-

ACPD
12, 7793–7827, 2012

tally. Therefore high resolution measurements are important for the understanding of the UTLS (e.g. Gettelman et al., 2011). Nevertheless, small and mesoscale structures and dynamical processes can seldom be observed in detail. In situ measurements require extensive planning and need to rely on forecasts (e.g. Pan et al., 2007). Satellites can only resolve structures with a large horizontal and vertical extent, i.e. a lower stratospheric intrusion was observed by HIRDLS (Olsen et al., 2008).

During the African Monsoon Multidisciplinary Analysis (AMMA) campaign (Redelsperger et al., 2006; Cairo et al., 2010), the CRyogenic Infrared Spectrometers and Telescope for the Atmosphere – New Frontiers (CRISTA-NF) was deployed on the high altitude aircraft M55-Geophysica (Stefanutti et al., 1999) which can reach a flight level of about 20 km. CRISTA-NF provides information about stratospheric and tropospheric trace gases with a vertical resolution of up to 500 m using the trace gas retrieval setup presented in Weigel et al. (2010). This enables CRISTA-NF to distinguish tropospheric and stratospheric air masses and to identify transport and mixing among them and hence, analyses of processes in the UTLS like e.g. blocking anticyclones or tropopause folds. This work presents CRISTA-NF measurements of H_2O, O_3, PAN, HNO_3, and temperature during the AMMA-SCOUT-O_3 flight on 29 July 2006. These CRISTA-NF measurements indicate an intrusion of stratospheric air into the troposphere with a horizontal resolution of few degree latitude.

CRISTA-NF observed structures in the distribution of trace gases which indicate that a tropopause fold was present in the vicinity of the subtropical jet. The jet itself inhibits horizontal transport but mixing is common in the regions around the jet (e.g. Gettelman et al., 2011). Intrusions and tropopause folds are often observed in connection with the jet streams and possibly give an important contribution to the stratosphere troposphere exchange (STE), (see, e.g. Shapiro, 1980; Seo et al., 2008; Olsen et al., 2008). Tracer-tracer correlations are a common way to analyze exchange processes between troposphere and stratosphere for in situ measurements and model simulations (e.g. Pan et al., 2004; James and Legras, 2007). Due to the narrow vertical field of view of CRISTA-NF (about 300 m at tangent height of 10 km, see Spang et al., 2008) and

ACPD
12, 7793–7827, 2012

a good vertical resolution of the observed trace gases, tracer-tracer correlations are applicable for the retrieval results to identify mixing.

Another method to learn more about the nature of processes in the atmosphere are model simulations. Lagrangian models are well suited to describe mesoscale processes. The Chemical Lagrangian Model of the Stratosphere (CLaMS; McKenna et al., 2002a,b) has been employed to analyze dynamical and chemical processes in the stratosphere and their influence on stratospheric trace gases. Several studies demonstrated the capability of CLaMS by comparing the simulation results to remote sensing measurements, among them the space shuttle experiment CRyogenic Infrared Spectrometers and Telescopes for the Atmosphere (CRISTA) (e.g. Khosrawi et al., 2005) and the Michelson Interferometer for Passive Atmospheric Sounding (MIPAS) (e.g. Vogel et al., 2008) and in situ data (e.g. Günther et al., 2008).

This work compares structures seen in the trace gas distributions retrieved from CRISTA-NF measurements to CLaMS model calculations and European Centre for Medium-Range Weather Forecasts (ECMWF) analysis data. In Sect. 2 the CRISTA-NF instrument and the CLaMS model are described, Sect. 3 presents the observed trace gases in comparison to the model results and Sect. 4 discusses observed structures and probable processes causing them.

2 Methods

2.1 The CRISTA-NF instrument

CRISTA-NF contains two mid infrared helium-cooled Ebert-Fastie grating spectrometer (Fastie, 1991) and a limb-viewing telescope. This optical system was originally part of the Space Shuttle experiment CRISTA (Offermann et al., 1999; Grossmann et al., 2002). During its two Space Shuttle missions, CRISTA detected numerous small and medium-scale transport and mixing structures in stratospheric trace gas distributions associated with exchange of tropical and extra-tropical air masses (e.g. Riese et

ACPD
12, 7793–7827, 2012

al., 1999, 2002). The aircraft version CRISTA-NF was deployed on the high-flying research aircraft M55-Geophysica (Stefanutti et al., 1999) during the SCOUT-O_3, AMMA-SCOUT-O_3, and RECONCILE measurement campaigns (e.g. Spang et al., 2008; Hoffmann et al., 2009; Weigel et al., 2010; Ungermann et al., 2011b). The helium cooled detectors and spectrometers allow a high signal to noise ratio and fast measurements. The field of view of CRISTA-NF is vertical narrow, about 300 m. One profile is measured in approximately 90 s corresponding to a horizontal distance of about 15 km along the flight track (Kullmann et al., 2004). A detailed description of the instrument can be found in Kullmann et al. (2004) the radiometric calibrations are explained in Schroeder et al. (2009).

The line of sight (LOS) points are located to the starebord-side of the aircraft. Most information originates from the tangent altitude, which is the altitude where the LOS is closest to the earth surface. Various satellite instruments use a similar observation geometry to retrieve profiles of atmospheric trace gases, e.g. MLS (Microwave Limb Sounder; see e.g. Waters et al., 2006) on Aura and MIPAS (Michelson Interferometer for Passive Atmospheric Sounding; see e.g. Fischer and Oelhaf, 1991) and SCIAMACHY (Scanning Imaging Absorption Spectrometer for Atmospheric CHartographY; see e.g. Bovensmann et al., 1999) on Envisat.

In the measurement mode used during the AMMA-SCOUT-O_3 campaign, an elevation mirror points the LOS to 60 different altitudes. This results in a profile of 60 measured spectra located between the aircrafts flight level and about 6 km altitude. The profiles lie slant in the atmosphere. This observation geometry with its high vertical sampling allows to retrieve data with a high vertical resolution aligned in a quasi-2D field. During the flight on the 29 July 2006 an active automated pointing stabilization was tested for the first time. It increased the pointing stability during each spectrum and produced more uniform vertical distances within each profile. This lead to a significantly improved data quality compared to the data presented in Hoffmann et al. (2009) and Weigel et al. (2010).

ACPD
12, 7793–7827, 2012

The JUelich Rapid Spectral Simulation Code (JURASSIC) (Hoffmann, 2006) is used to retrieve the composition of the atmosphere. The retrieval algorithm used is based on the optimal estimation maximum a posteriori approach, see Rodgers (2000). JURASSIC was applied previously for the retrieval of data from several satellites (Hoffmann et al., 2008; Hoffmann and Alexander, 2009) and CRISTA-NF (Hoffmann et al., 2009; Weigel et al., 2010). The used retrieval setup allows to retrieve altitude, temperature, and the volume mixing ratios of water vapor (H_2O), ozone (O_3), nitric acid (HNO_3), peroxyacetyl nitrate (PAN), carbon tetrachloride (CCl_4) as well as aerosol extinction and a radiometric offset. The setup is explained in detail in Weigel et al. (2010), where a tropical CRISTA-NF flight was discussed. Because the flight presented here took place in the extra tropics at about 40° N the mid latitude value from the climatology of Remedios et al. (2007) are used for most trace gases. This differs from Weigel et al. (2010), where the tropical value from the climatology was used as a priori or fixed value for several trace gases and Atmospheric Chemistry Experiment – Fourier Transform Spectrometer (ACE-FTS) data were used as fixed value for HCFC−22. For the setup used here, reliable informations about CFC-11 and CFC-12 are important for the altitude and temperature retrieval. As in Weigel et al. (2010), CFC-11 and CFC-12 profiles measured on the current flight by the High Altitude Gas Analyser (HAGAR) instrument (see e.g. Werner et al., 2010 and Homan et al., 2010) are combined with climatological mixing ratios from Remedios et al. (2007). A priori profiles for O_3 and temperature, and informations about wind speed and potential vorticity are taken from interpolated ECMWF operational analysis data with 0.5 degrees horizontal resolution on 28 pressure levels interpolated on the retrieval grid and position for each profile.

Spectra with optical dense conditions need to be excluded from the retrieval. Optical dense conditions are defined by the cloud index (CI),the ratio of the mean radiances at 791–793 and 830–832 $cm^{-}1$, (Spang et al., 2008)). When the CI is lower than the threshold value of 3.5 no retrieval is done. In most cases optical dense conditions are caused by clouds. To display the information of the cloud position together with the

ACPD
12, 7793–7827, 2012

retrieved trace gases, the tangent points of spectra with optical dense conditions are corrected for the result of the altitude retrieval and refraction.

2.2 The CLaMS model

Data from the Chemical Lagrangian Model of the Stratosphere (CLaMS; McKenna et al., 2002a,b) have been compared to the CRISTA-NF observations. The introduction of a hybrid vertical coordinate (ζ-coordinates, see Konopka et al., 2007) extended the range of application for CLaMS to the tropopause region and troposphere where most of the CRISTA-NF measurements are located. The $\zeta-$coordinates are a combination between potential temperature in the stratosphere and pressure in the troposphere,

The CLaMS model run used in this study is a two month transient global run embedded in a climatological run following Konopka et al. (2007) using the HALOE climatology developed by Grooß and Russell (2005) for initialization and boundary conditions for most trace gases. For H_2O ECMWF analysis data are used for initialization and boundary conditions. Lower and upper boundaries are set to ζ =200 K and ζ =500 K, respectively. Condensation and freezing are based on cloud parameters by Krämer et al. (2008) and Schiller et al. (2008). The horizontal resolution is 70 km between 20 and 40° N and 100 km north and south of this latitude range. CLaMS was run with a temporal resolution of 6 h and a Lyapunov exponent of 1.5. To adjust the time between CRISTA-NF observations and CLaMS fields a correction based on the CLaMS trajectories is used.

Since the vertical resolution of CLaMS is partly better than the vertical resolution of CRISTA-NF, CLaMS data are interpolated onto the CRISTA-NF grid and their resolution is degraded with the Averaging Kernel (AVK) of CRISTA-NF, following e.g. von Clarmann (2006). This ensures that the CLaMS data, like the a priori data used for comparison in Weigel et al. (2010) are comparable to the CRISTA-NF retrieval results in terms of resolution and a priori influence.

ACPD
12, 7793–7827, 2012

3 Results and comparisons

3.1 The AMMA flight on 29 July 2006

This work concentrates on the AMMA flight on 29 July 2006, which took place over Italy and the Mediterranean Sea. Figure 1 shows the H_2O and O_3 distributions on the 350 K level from the CLaMS simulation between 10° N–60° N and 60° E–60° W. Different potential vorticity value are used in the literature to represent the dynamical tropopause, the best choice is in principle dependent on location and season (Gettelman et al., 2011). In Fig. 1 the 2 and 4 PVU (potential vorticity units) line from ECMWF are displayed to indicate where the 350 K level intersects the dynamical tropopause. In this area, the 350 K level is located partly in the troposphere and partly in the stratosphere: North of the 2 and 4 PVU lines air of stratospheric characteristics, i.e. high O_3 and low H_2O mixing ratios prevail while the 350 K level is located in the troposphere to the south of both PVU lines. Areas with horizontal wind speed of more than 25 and 35 m s^{-1} are marked to show the position of the subtropical jet.

The 2 and 4 PVU line are separated by more than 10° Latitude over parts of the North Atlantic but lie close together over the central Mediterranean Sea and Eastern Europe. This indicates a sharp transition between the lowermost stratosphere in the north and the troposphere in the south on the 350 K level. This transition region was crossed twice during the flight over the Mediterranean Sea. The subtropical jet, marked by the 25 and 35 m s^{-1} contour line of the ECMWF wind speed, is most often found close to the 4 PVU line. Over the Atlantic it is situated further north at about 45° N than over and east of the Mediterranean Sea, where it is at about 35° to 40° N. Water vapor mixing ratios of more than 20 ppmV are found nearly everywhere south of the 2 PVU line and at some places between 2 and 4 PVU. North of the 4 PVU line the water vapor mixing ratios are usually lower than 15 ppmV. On contrary high O_3 mixing ratios (usually above 250 ppbV) are found north of the 4 PVU line. South of the 2 PVU line the O_3 mixing ratios are mostly lower than 200 ppbV. Between the 2 and the 4 PVU line intermediate O_3 mixing ratios (200–250 ppbV) are found.

ACPD
12, 7793–7827, 2012

The flight track is located over Italy and the central Mediterranean Sea, where the 2 and 4 PVU lines lie close together and where a narrow core of the jet with a wind speed of more than 35 m/s occurred. The flight track is shown in the inlay of Fig. 2. Starting in Verona, the M55-Geophysica flew to the south-east. North of the coast of Sicily, after three short legs towards east, southwest and west the aircraft turned and returned to Verona. A dive down to about 9 km was performed on the legs towards southwest and west. The view direction of CRISTA-NF is to the right of the aircraft, thus the measurements during the southeastward leg were taken over the Mediterranean Sea. On the way back to Verona they were taken above Italy and the Adriatic Sea. During the turn north of Sicily CRISTA-NF views towards southeast over Sicily and in northward directions during the dive.

The main part of Fig. 2 displays a three-dimensional view of the flight path and schematic representation of the CRISTA-NF retrieval grid including the horizontal position of the closest tangent point. Black dots show spectra with optical dense conditions due to clouds. Large parts of the flight were performed in cloud free air down to an altitude of 8 km providing excellent conditions for trace gas retrievals.

Colored symbols represent the CRISTA-NF PAN measurements positioned on the retrieval grid (vertical) and at the horizontal position of the nearest tangent point (including the effect of refraction). The vertical extent of these symbols denotes the vertical resolution of the retrieval result. The vertical resolution is calculated according to the method proposed by Purser and Huang (1993). Due to the nature of the limb measurements the horizontal resolution is much coarser, in the order of several 100 km (see Ungermann et al., 2011b for a more detailed discussion). Another measure for the quality of the retrieval is the measurement contribution. It approximates contribution of the measurement relative to the contribution of the a prior values to the retrieval result. To assess the quality of the retrieved data the measurements contribution, the $\chi^2\,\mathrm{m}^{-1}$ values, and the resolution are calculated as described in Weigel et al. (2010). All CRISTA-NF results shown are filtered for measurement contribution between 0.8 and 1.2 and a resolution better than 5 km. Fewer data were analyzed during the dive

ACPD
12, 7793–7827, 2012

because of increased aircraft movements and hence decreased data quality (causing the white areas in the middle of the retrieval results in Figs. 3–5).

3.2 Water vapor and clouds

Figure 3 shows the water vapor mixing ratios retrieved from CRISTA-NF (panel a), from the CLaMS simulation (panel b), and from ECMWF (panel c). The ECMWF and CLaMS data are interpolated on the grid shown in Fig. 2 and folded with the AVK to be comparable to the CRISTA-NF data with respect to a priori influence and resolution. In addition to the 2 and 4 PVU lines from ECMWF shown in Fig. 1, the 1.5 PVU line is displayed in Fig. 3 and the following vertical cross sections. The 1.5 PVU line does not follow the 2 PVU line with a constant vertical distance but shows an even steeper increase and decrease in altitude at about 07:15 and 08:15 UTC, respectively. The flight altitude and the PVU lines are shown in all panels for better comparison. Additionally, the spectra with optical dense conditions are marked (panel a). As in Weigel et al. (2010), a climatological profile was chosen as a priori for H_2O in the retrieval to ensure that all variations are a result of the measurements and not influenced by the choice of the a priori value.

The detection limit for CRISTA-NF H_2O is about 15 ppmV. For lower H_2O mixing ratios the combined error exceeds 90 %. Here, the detection limit is reached above 12.5 km altitude for most profiles. An exception are single, remarkably high water vapor values at altitudes of 13-14 km found in two isolated structures at about 7:00 and 8:30 UTC as well as enhanced H_2O mixing ratios in this altitude in the southernmost part of the flight, between 07:15–08:15 UTC. Below 12 km the H_2O mixing ratios are lowest in the southernmost part of the flight.

At 12 to 13 km altitude, there is an enhanced amount of water vapor mixing ratio in the southernmost part of the flight between about 07:15 to 08:15 UTC in the CLaMS data. This agrees in general with the CRISTA-NF results but the CLaMS H_2O mixing ratios are somewhat higher and more uniform at these altitudes. The structures of enhanced water vapor seen at about 07:00 and 08:30 UTC in the CRISTA-NF results

ACPD
12, 7793–7827, 2012

above 12 km are not found in the CLaMS data. As in the CRISTA-NF data, there is less water vapor in the southern part of the flight than in the northern part for the CLaMS data at lower altitudes. But for CLaMS this is the case for altitudes below 10 km and not up to 12 km as for CRISTA-NF. Below 12 km altitude the CLaMS water vapor mixing ratios are lower than the retrieved ones almost everywhere.

The ECMWF H_2O mixing ratios agree well with the CRISTA-NF results below 12 km. However, the enhanced water vapor values and horizontal structures seen by CRISTA-NF and CLaMS above 12 km are not found in the ECMWF data. For ECMWF the water vapor is lowest in the south (i.e. between about 07:00 and 08:30 UTC) for all altitudes up to 14 km.

3.3 Ozone

The O_3 mixing ratios from CRISTA-NF, CLaMS, and ECMWF are shown in Fig 4. In general, the O_3 mixing ratio increases with altitude. In all panels low, tropospheric O_3 mixing ratios are found up to 15 km altitudes in the middle of the plot, i.e. the southern part of the flight track between about 07:00 and 08:30 UTC. Here, also the 1.5, 2 and 4 PVU lines from ECMWF are found about 2–3 km higher than in the northern part of the flight (i.e. before 07:00 and after 08:30 UTC). The altitudes, shape and absolute O_3 mixing ratios differ between the different data sets. It is important to note that the low ozone mixing ratios at altitudes up to 13.5–16 km are not part of an enclosed feature. The aircraft is turning before 08:00 UTC, measuring the same structure a second time. This time the viewing direction is now toward the northeast instead of southwest.

For the CRISTA-NF data (Fig. 4a) O_3 mixing ratios lower than 200 ppbV are found up to an altitude of 16 km in the southern part of the flight track between about 07:00 and 08:30 UTC. There, the vertical gradient between tropospheric and stratospheric O_3 mixing ratios is especially steep, whilst it is much smoother in the northern part of the flight track. The vertical gradient is smoothest within two intrusions of air with high, rather stratospheric O_3 mixing ratios into the troposphere in between. These structures observed in the O_3 mixing ratios are significant compared to the size of the retrieval

ACPD
12, 7793–7827, 2012

errors. There are somewhat higher O_3 mixing ratios in the first half of the flight than in the second half, but in general the structures are nearly symmetrical in both flight directions. This indicates a structure with several hundred kilometers horizontal extent (> 600 km) perpendicular to the flight track. The horizontal extent along the flight track is about 350 km.

In the first half of the flight there are large O_3 mixing ratios reaching down to below 10 km, at about 06:40 UTC. This is, if at all, only mirrored by a single profile at about 08:50 UTC in the second half of the flight. Another region with enhanced O_3 is present directly in the beginning of the flight, down to about 11 km. It is not found in the second half, presumably because the descent of the aircraft starts before.

A comparison of the structure found in the O_3 in Fig. 4a to the retrieved water vapor in Fig 3a shows that the isolated structures of enhanced H_2O observed at 07:00 and 08:30 UTC above 12 km coincide with the base of the intrusion of stratospheric O_3.

The vertical O_3 distribution from CLaMS (Fig. 4b) has a very similar shape compared to the one measured by CRISTA-NF. O_3 with less than 200 ppbV is found up to an altitude of 15.5 km in the southern part of the flight track and there are also intrusions with enhanced O_3 and a smooth transition between low and high O_3 mixing ratios in between the southern and the northern part. The absolute O_3 values differ between CLaMS and CRISTA-NF. In regions of low O_3 CRISTA-NF is lower by 50–100 ppbV than CLaMS in most places, about 200 ppbV in maximum. Above, where higher O_3 volume mixing ratios are found the CRISTA-NF data are about 50–250 ppbV higher than the CLaMS results.

For the ECMWF data (Fig. 4c) the transition is rather smooth and the gradient between low and high O_3 about the same along the whole flight path. O_3 with less than 200 ppbV is found highest at about 14.5 km. The intrusion of stratospheric air into the troposphere seen in the CRISTA-NF and CLaMS O_3 mixing ratios is not found in the ECMWF data.

ACPD
12, 7793–7827, 2012

3.4 Other trace gases and temperature

The CRISTA-NF mixing ratios for HNO_3 and PAN as well as temperature are shown in Fig. 5. HNO_3 has a similar structure as O_3 for the southern part of the flight (i.e. before 07:00 and after 08:30 UTC), while for the northern part the gradient between HNO_3 mixing ratios within stratospheric and tropospheric air is more smooth than for O_3. Like O_3, HNO_3 has a higher mixing ratio in the stratosphere than in the troposphere.

PAN is a tracer originating from the troposphere mainly from aged pollution. The lifetime of PAN is in the order of months in the upper troposphere (Talukdar et al., 1995). Its vertical structure during this flight is similar to the one observed for H_2O. For PAN the detection limit for CRISTA-NF measurements is at about 50 pptV. This is usually reached in the lower stratosphere above about 16 km for most of the profiles. In the southern part PAN mixing ratios of about 80 pptV are found up to 15.5 km altitude, in the northern part these values are rather located at 14 km. Enhanced mixing ratios of PAN with over 150 pptV are also found at the same location as the enhanced H_2O obvious in Fig. 3 at 07:00 and 08:30 UTC between about 12 and 13.5 km. There is an isolated maximum at 07:15 and 08:15 UTC in the 14–15 km region with over 125 pptV PAN surrounded by air with lower PAN mixing ratios of about 90 pptV. The distribution is quasi symmetric for the southward and northward flight leg, but the absolute values are higher during the first half of the flight, i.e. with the LOS pointing westward. For both HNO_3 and PAN the observed structures are in most cases significant compared to the combined retrieval error.

Figure 5c shows the temperature retrieved from CRISTA-NF observations. The lowest temperatures for each profile are found at altitudes between 16 and 18 km during the whole flight. The minimum temperature along the flight path, about 205 K, is located at about 16 to 17 km altitude in the southernmost profiles (at about 07:30 UTC). In this part of the flight also the highest temperatures are observed at an altitude below about 10 km. Thus, the temperature gradient is steeper in the southern part, as expected for

ACPD
12, 7793–7827, 2012

air masses of tropical origin. In the northernmost part of the flight, a local minimum can be seen at a altitude of about 12 to 12.5 km.

In summary the trace gases retrieved from CRISTA-NF measurements show a transition from stratospheric to tropospheric characteristics between about 10 and 15 km altitude at the position where the height of the thermal and dynamical tropopause increases and the subtropical jet is located. This transition is not as clear in the ECMWF data and does not reach as high up as seen in the measurements. The shape and position of the vertical O_3 distribution is reproduced well in the CLaMS simulation although the tropospheric O_3 mixing ratios are not as low as the ones observed by CRISTA-NF.

4 Discussion

The detailed observation of the transition between stratospheric and tropospheric air at the subtropical jet raises the questions where the observed air masses originate from, whether mixing occurs between them and what kind of structure is observed.

4.1 Where do the observed air masses originate from?

To gain further insight into the origin and the fate of the air masses detected during the flight trajectories are calculated with CLaMS. Figure 6 shows 10 days backward trajectories of air parcels arriving at all CRISTA-NF grid positions between 350 and 360 K ζ. For ζ between 350 and 360 K relatively low O_3 values are only found in the southern part of the flight. The trajectories reveal that nearly all air parcels with low O_3 volume mixing ratios lower than 200 ppbV originate from the region around the Asian monsoon anticyclone. In contrast, about all trajectories arriving at the northern part of the flight track with O_3 values higher than 200 ppbV come from westward directions along the subtropical jet.

The low O_3 and HNO_3 mixing ratios along with high PAN mixing ratios in the southern part of the flight also correspond well to ACE-FTS observations of low O_3 and HNO_3

ACPD
12, 7793–7827, 2012

and high mixing ratios of tropospheric species within the Indian monsoon anticyclone (Park et al., 2008). They observe a strong isolation of the air within this anticyclone. Air influence by the Indian monsoon is also found by Barret et al. (2008) in MLS CO measurements over the Mediterranean Sea in July 2006.

To get a deeper insight on the vertical distribution of the observed trace gases, Fig. 7 shows scatter plots of O_3 and PAN versus potential temperature calculated from CRISTA-NF temperature measurements and ECMWF analysis pressure. The altitude where the data is observed is color coded. For a potential temperature above about 400 K O_3 increases strong and approximately linearly, as expected for stratospheric air. These values are found at altitudes of 16 km or higher. Below 400 K the spread of observed O_3 mixing ratios is wider. At 370 K both tropospheric mixing ratios lower than 100 ppbV and mixing ratios influenced by stratospheric air up to 300 ppbV occur. Their altitude varies between up to 16 km for the tropospheric mixing ratios and about 14 km for rather stratospheric mixing ratios. This shows, that during these measurements tropospheric mixing ratios where observed at higher altitudes than stratospheric mixing ratios. Reasons are, that the height of the tropopause varies along the flight track and transport processes between stratosphere and troposphere occur, as it can be expected near the subtropical jet (e.g. Gettelman et al., 2011). The distribution of PAN versus potential temperture differs from the one of O_3. The main source of PAN is in the troposphere. Therefore the highest PAN mixing ratios are found below 350 K and 12 km. Above 380 K PAN mixing ratios decrease linearly with increasing potential temperature.

4.2 Do the observed air masses mix?

As shown in Fig. 7, the vertical gradients of stratospheric and tropospheric trace gases like O_3 have the opposite sign as the gradients of tropospheric trace gases. Therefore, mixing at the tropopause is often identified by tracer-tracer correlations, especially for in situ measurements, e.g. Hoor et al. (2002) and Pan et al. (2004). Hegglin (2010) uses

ACPD
12, 7793–7827, 2012

tracer-tracer correlations to identify the extratropical transition layer (exTL), a layer with mixed tropospheric and stratospheric air, from ACE-FTS measurements.

The CRISTA-NF observations of PAN are of better quality than the H_2O observations due to their lower instrumental error and detection limit. In addition to dynamical processes the transport of H_2O between the troposphere and the stratosphere is influenced by microphysical processes in connection with clouds, like condensation, evaporation, freezing, and sublimation. Therefore PAN is a better tracer for the mixing of tropospheric and stratospheric air masses. Hence, PAN is used here as tropospheric trace gas for the tracer-tracer correlation with O_3 (Fig. 8a). Between the low PAN and high O_3 values above 14 km and the high PAN and low O_3 below 13 km there are intermediate values found between about 10 and 14 km. Such measurements with more than 100 ppbV O_3 and simultaneously more than 120 pptV PAN indicate mixing between tropospheric and stratospheric air and are marked with pink circles in Fig. 8. Like Hegglin (2010), we use 100 ppbV as threshold value for tropospheric O_3. On the contrary, according to Fig. 7 O_3 mixing ratios up to 160 ppbV are observed for the lowest potential temperatures and altitudes.

The altitudes where intermediate PAN and O_3 mixing ratios occur, indicate a layer about 4 km wide with mixing between tropospheric and lowermost stratospheric air. It is similar to the one found by Pan et al. (2007) in connection with a tropopause fold on the cyclonic side of the polar jet in December 2005, using in situ measurements. Pan et al. (2007) observed a depth of the mixed air up to 5 km with rather low O_3 values with 100 ppbV also within the mixed air. For the CRISTA-NF measurements during the flight on 29 July the O_3 mixing ratios within the mixed air is significantly higher (up to 300 ppbV).

4.2.1 How does the resolution of CRISTA-NF influence the observations?

Due to the limb viewing geometry the measurements of CRISTA-NF provide an integrated information along the lines of sight. It certainly helped to resolve the observed structure that the flight track was aligned nearly perpendicular to it, providing that the

ACPD
12, 7793–7827, 2012

CRISTA-NF measurements also have a relatively high horizontal resolution and sampling in addition to the generally high vertical resolution. For the altitudes where the mixing is observed the vertical resolution of PAN and O_3 is in most cases better than 3 km. Values with coarser resolution are marked with grey stars in Fig. 8a. Often, the resolution is better than 2 km for O_3 and 1 km for PAN.

Unlike in situ measurements CRISTA-NF provides a quasi-2D cross sections of the atmosphere. Therefore, no in situ measurements deployed on the M55-Geophysica during this flight would be able to detect these structures without extensive flight maneuvers at lower altitudes, which would require some predictive knowledge of the structure.

Hegglin (2010) argued that for ACE-FTS, which has a similar observation geometry but from space, it is extremely unlikely, that air from lower altitudes than the tangent point is observed along the LOS. Therefore the high values of PAN above 12 km (Fig. 5) can not be caused by the measurement geometry or the extent of the field of view. It is possible, that the retrieved tropospheric O_3 values are increased due to the influence of higher stratospheric O_3 above, but these influence should be about the same for all values in the same altitude. Hence, horizontal gradients should not be influenced. Because mixed and not mixed air is found within the same altitudes and because the layer with mixed air is wider than 4 km, the observed mixing can not be only an artifact of the resolution.

The limb geometry and the field of view of CRISTA-NF may lead to an overestimation of mixing due to enhanced values of stratospheric trace gases and it can be expected that structures have an even smaller vertical extent than seen by the measurements. For this reason it is not possible to give a quantitative estimate of the mixing between stratospheric and tropospheric air or decide if the intrusion of stratospheric air into the troposphere is reversible or irreversible. This can be facilitated by potential future satellite missions, which can provide a similar sampling and spectral resolution as CRISTA-NF with on a global coverage.

ACPD
12, 7793–7827, 2012

4.3 What kind of structure is observed?

To get a better insight in the kind of structure that was observed, Fig. 8 resembles the information obtained from CRISTA-NF, CLaMS and ECMWF along the flight path. The gray lines show the 1.5, 2 and 4 PVU surfaces as taken from the ECMWF data, the black line shows the flight altitude. The position of the subtropical jet is marked by golden contour lines showing the horizontal wind speed from ECMWF. Light blue diamonds show the laps-rate (or thermal) tropopause calculated from CRISTA-NF measurements following the WMO definition. The laps-rate tropopause lays at about 11–12 km in the northern and at about 16 km in the southern part of the flight. At 07:00 and 08:45 there is a jump in the altitude of the thermal tropopause of about 4 km. ζ-levels from CLaMS are shown as red contours. The measurements indicating mixed air from Fig. 8a are again marked as pink circles in Fig. 8b.

The dynamical tropopause, often defined as the 2 PVU surface (e.g. Pan et al., 2004), is situated at about 10 km altitude in the northern part of the flight. During the southern part the 2 PVU surface is located somewhat higher up, at about 13 km. during most of the flight the lapse-rate tropopause is located above the 4 PVU surface (agreeing well with the findings of Kunz et al., 2009). The vertical and meridional wind speeds in the ECMWF data show that the rise of the 2 PVU surface and the shift in the thermal tropopause from low to high altitudes is located precisely at the center of the subtropical jet. Figure 8b shows that the mixed air identified by the tracer-tracer correlation in Fig. 8a is found at the northern side of the jet up to about 14.5 km altitude and $\zeta = 380$ K and at up to about 13 km further northwards in the lowermost stratosphere (above the 2 PVU line and around the laps-rate tropopause).

Shapiro (1980) described tropopause folds as mixing regions characterized by a chemical characterization between troposphere and stratosphere. The 2 PVU surface in the ECMWF data is not folded as sharply as one might expect in this case, but one should remember that the O_3 intrusion seen in the CRISTA-NF measurements is not resolved in the ECMWF data, too. Nevertheless, all PVU surfaces shown in Fig. 8 rise

ACPD
12, 7793–7827, 2012

at least 2 km, where the O_3 intrusion is observed by CRISTA-NF. Also the relatively high O_3 values in the northern part of the flight down to below 10 km concur with decreasing altitudes of the shown PVU surfaces. In the ECMWF O_3 (Fig. 4c) no corresponding structure is present. These results indicate that the CRISTA-NF measurements show a detailed cross section through a tropopause fold.

Tropopause folds are suspected to be one of the main mechanisms for cross-tropopause-transport (e.g. Shapiro, 1980 and Seo et al., 2008). Hoor et al. (2002) observed a greater depth of the mixing layer above the extra-tropical tropopause during summer and explained it with transport across the tropopause at the subtropical jet. Mixing between tropospheric and lower stratospheric air is observed to occur often in connection with tropopause folds (e.g. Gettelman et al., 2011 and references therein).

In summary, the results of the AMMA flight on 29 July 2006 show that CRISTA-NF provides detailed measurements in the UTLS. The data obtained agree well with modeled data from CLaMS. CRISTA-NF observations and CLaMS simulations indicate, that a tropopause fold was observed, which was not resolved by the ECMWF operational analysis.

5 Conclusions and outlook

Utilizing the retrieval setup presented in Weigel et al. (2010) a detailed analysis is performed for the flight on 29 July 2005. CRISTA-NF data provides a detailed, two dimensional insight into the UTLS, measuring both trace gases of tropospheric and stratospheric origin. This allows to observe and analyze mesoscale processes. Better understanding of mesoscale processes has implications for the medium range weather forecast and ozone chemistry (WMO, 2006). A sharp transition between tropospheric and stratospheric air was observed over the Mediterranean Sea, identified by strong gradients in O_3, HNO_3, and PAN. The structure was reproduced by CLaMS simulations but was not completely resolved in the ECMWF operational analysis data set.

ACPD
12, 7793–7827, 2012

It is most probable that the observed intrusion of stratospheric air into the troposphere is the result of a tropopause fold, which is not well resolved in the ECMWF data. CLaMS simulations made it possible to gain further information about the origin and the fate of the observed air masses. They indicate that the observed air originated on the one hand from the tropopause close to the Asian monsoon anticyclone and on the other hand in the extra tropical lowermost stratosphere along the subtopical jet. Tracer-tracer correlations between PAN and O_3 retrieved from the CRISTA-NF measurements show the presence of mixed tropospheric and stratospheric air. This emphasizes that vertically high resolved limb soundings are capable to provide a detailed picture of the chemical composition in the UTLS.

To investigate the UTLS in such detail on a global scale could help to gain a better understanding of the whole atmosphere. This could be achieved in the future by limb-imaging spectrometers as Imaging spectrometers as the GLObal limb Radiance Imager for the Atmosphere (GLORIA), see e.g. Riese et al., 2005; Friedl-Vallon et al., 2006). An air-borne version of this intrument, GLORIA-AB (Gimballed Limb Observer for Radiance Imaging of the Atmosphere, airborne version) has been developed for the High Altitude and Long Range Research Aircraft (HALO) and M55-Geophysica aircraft. The instrument was successfully tested on M55-Geophysica in December 2011. GLORIA-AB will provide an even better resolved view of such small scale structures (Ungermann et al., 2011a). GLORIA-AB serves as a prototype for a next generation satellite-borne limb-imager like the ESA candidate mission PREMIER (PRocesses Exploration through Measurements of Infrared and millimeter-wave Emitted Radiation, ESA, 2008; Ungermann et al., 2010). This instrument can offer the possibility to provide global observations of small- and mesoscale processes and quantify their effect on the total exchange between troposphere and stratosphere.

Acknowledgements. The AMMA-SCOUT-O3 measurement campaign was facilitated by the European Commission and the EC Integrated Project SCOUT-O3 (505390-GOCE-CT-2004) and AMMA. Based on a French initiative, AMMA was set up by an international scientific group and is currently funded by a large number of agencies. It has been the beneficiary of a major

ACPD
12, 7793–7827, 2012

financial contribution from the European Communities Sixth Framework Research Program. Many thanks also to the team and pilots of the Myasishchev Design Bureau for making the M55-Geophysica flights possible under difficult logistic conditions. For providing observation data from HAGAR for retrieval support we like to thank C. M. Volk. Last but not least we like to thank everybody, who provided technical support for the CRISTA-NF measurements and data analysis.

References

Barret, B., Ricaud, P., Mari, C., Attié, J.-L., Bousserez, N., Josse, B., Le Flochmoën, E., Livesey, N. J., Massart, S., Peuch, V.-H., Piacentini, A., Sauvage, B., Thouret, V., and Cammas, J.-P.: Transport pathways of CO in the African upper troposphere during the monsoon season: a study based upon the assimilation of spaceborne observations, Atmos. Chem. Phys., 8, 3231–3246, doi:10.5194/acp-8-3231-2008, 2008. 7807

Bovensmann, H., Burrows, J. P., Buchwitz, M., Frerick, J., Noël, S., Rozanov, V. V., Chance, K. V., and Goede, A. P. H.: SCIAMACHY: Mission objectives and measurement modes, J. Atmos. Sci., 56, 127–149, 1999. 7797

Cairo, F., Pommereau, J. P., Law, K. S., Schlager, H., Garnier, A., Fierli, F., Ern, M., Streibel, M., Arabas, S., Borrmann, S., Berthelier, J. J., Blom, C., Christensen, T., D'Amato, F., Di Donfrancesco, G., Deshler, T., Diedhiou, A., Durry, G., Engelsen, O., Goutail, F., Harris, N. R. P., Kerstel, E. R. T., Khaykin, S., Konopka, P., Kylling, A., Larsen, N., Lebel, T., Liu, X., MacKenzie, A. R., Nielsen, J., Oulanowski, A., Parker, D. J., Pelon, J., Polcher, J., Pyle, J. A., Ravegnani, F., Rivière, E. D., Robinson, A. D., Röckmann, T., Schiller, C., Simões, F., Stefanutti, L., Stroh, F., Some, L., Siegmund, P., Sitnikov, N., Vernier, J. P., Volk, C. M., Voigt, C., von Hobe, M., Viciani, S., and Yushkov, V.: An introduction to the SCOUT-AMMA stratospheric aircraft, balloons and sondes campaign in West Africa, August 2006: rationale and roadmap, Atmos. Chem. Phys., 10, 2237–2256, doi:10.5194/acp-10-2237-2010, 2010. 7795

European Space Agency: PREMIER: Candidate Earth Explorer Core Missions – Reports for Assessment, ESA SP-1313(5), Mission Science Division, ESA-ESTEC, Noordwijk, The Netherlands, ISSN 0379–6566, 121 pp., 2008. 7812

Fastie, W. G.: Ebert Spectrometer Reflections, Phys. Today, 4, 37–43, 1991. 7796

ACPD
12, 7793–7827, 2012

Fischer, H. and Oelhaf, H.: Remote sensing of vertical profiles of atmospheric trace constituents with MIPAS limb-emission spectrometers, Appl. Opt., 35, 2787–2796, 1996. 7797

Friedl-Vallon, F., Riese, M., Maucher, G., Lengel, A., Hase, F., Preusse, P., and Spang, R.: Instrument concept and preliminary performance analysis of GLORIA, Adv. Space Res., 37, 2287–2291, 2006. 7812

Gettelman, A., Hoor, P., Pan, L. L., Randel, W. J., Hegglin, M. I., and Birner, T.: The extratropical upper troposphere and lower stratosphere, Rev. Geophys., 49, RG3003, doi:10.1029/2011RG000355, 2011. 7795, 7800, 7807, 7811

Grooß, J.-U. and Russell III, J. M.: Technical note: A stratospheric climatology for O3, H2O, CH4, NOx, HCl and HF derived from HALOE measurements, Atmos. Chem. Phys., 5, 2797–2807, doi:10.5194/acp-5-2797-2005, 2005. 7799

Grossmann, K. U., Offermann, D., Gusev, O., Oberheide, J., Riese, M., and Spang, R.: The CRISTA-2 mission, J. Geophys. Res., 107, 8173, doi:10.1029/2001JD000667, 2002. 7796

Günther, G., Müller, R., von Hobe, M., Stroh, F., Konopka, P., and Volk, C. M.: Quantification of transport across the boundary of the lower stratospheric vortex during Arctic winter 2002/2003, Atmos. Chem. Phys., 8, 3655–3670, doi:10.5194/acp-8-3655-2008, 2008. 7796

Hegglin, M. I., Gettelman, A., Hoor, P., Krichevsky, R., Manney, G. L., Pan, L. L., Son, S.-W., Stiller, G., Tilmes, S., Walker, K. A., Eyring, V., Shepherd, T. G., Waugh, D., Akiyoshi, H., Añel, J. A., Austin, J., Baumgaertner, A., Bekki, S., Braesicke, P., Brühl, C., Butchart, N., Chipperfield, M., Dameris, M., Dhomse, S., Frith, S., Garny, H., Hardiman, S. C., Jöckel, P., Kinnison, D. E., Lamarque, J. F., Mancini, E.,Michou,M., Morgenstern, O., Nakamura, T., Olivié, D., Pawson, S., Pitari, G., Plummer, D. A., Pyle, J. A., Rozanov, E., Scinocca, J. F., Shibata, K., Smale, D., Teyssèdre, H., Tian, W., Yamashita: Multimodel assessment of the upper troposphere and lower stratosphere: Extratropics, J. Geophys. Res., 115, D00M09, doi:10.1029/2010JD013884., 2010. 7807, 7808, 7809

Hoffmann, L.: Schnelle Spurengasretrieval für das Satellitenexperiment Envisat MIPAS, PhD thesis, University of Wuppertal, 2006. 7798

Hoffmann, L., Kaufmann, M., Spang, R., Müller, R., Remedios, J. J., Moore, D. P., Volk, C. M., von Clarmann, T., and Riese, M.: Envisat MIPAS measurements of CFC-11: retrieval, validation, and climatology, Atmos. Chem. Phys., 8, 3671–3688, doi:10.5194/acp-8-3671-2008, 2008. 7798

ACPD
12, 7793–7827, 2012

Hoffmann, L., M. J. Alexander: Retrieval of Stratospheric Temperatures from Atmospheric Infrared Sounder Radiance Measurements for Gravity Wave Studies, J. Geophys. Res., 114, D07105, doi:10.1029/2008JD011241, 2009. 7798

Hoffmann, L., Weigel, K., Spang, R., Schroeder, S., Arndt, K., Lehmann, C., Kaufmann, M., Ern, M., Preusse, P., Stroh, F., Riese, M.: CRISTA-NF measurements of water vapor during the SCOUT-O3 Tropical Aircraft Campaign, Adv. Space Res., 43, 74–81, 2009. 7797, 7798

Homan, C. D., Volk, C. M., Kuhn, A. C., Werner, A., Baehr, J., Viciani, S., Ulanovski, A., and Ravegnani, F.: Tracer measurements in the tropical tropopause layer during the AMMA/SCOUT-O3 aircraft campaign, Atmos. Chem. Phys., 10, 3615–3627, doi:10.5194/acp-10-3615-2010, 2010. 7798

Hoor, P., H. Fischer, L. Lange, J. Lelieveld, and D. Brunner: Seasonal variations of a mixing layer in the lowermost stratosphere as identified by the CO-O_3 correlation from in situ measurements, J. Geophys. Res., 107, 4044, doi:10.1029/2000JD000289, 2002. 7807, 7811

James, R. and Legras, B.: Mixing processes and exchanges in the tropical and the subtropical UT/LS, Atmos. Chem. Phys., 9, 25–38, doi:10.5194/acp-9-25-2009, 2009. 7795

Khosrawi, F., Grooß, J.-U., Müller, R., Konopka, P., Kouker, W., Ruhnke, R., Reddmann, T., and Riese, M.: Intercomparison between Lagrangian and Eulerian simulations of the development of mid-latitude streamers as observed by CRISTA, Atmos. Chem. Phys., 5, 85–95, doi:10.5194/acp-5-85-2005, 2005. 7796

Konopka, P., Günther, G., Müller, R., dos Santos, F. H. S., Schiller, C., Ravegnani, F., Ulanovsky, A., Schlager, H., Volk, C. M., Viciani, S., Pan, L. L., McKenna, D.-S., and Riese, M.: Contribution of mixing to upward transport across the tropical tropopause layer (TTL), Atmos. Chem. Phys., 7, 3285–3308, doi:10.5194/acp-7-3285-2007, 2007. 7799

Krämer, M., Schiller, C., Afchine, A., Bauer, R., Gensch, I., Mangold, A., Schlicht, S., Spelten, N., Sitnikov, N., Borrmann, S., de Reus, M., and Spichtinger, P.: Ice supersaturations and cirrus cloud crystal numbers, Atmos. Chem. Phys., 9, 3505–3522, doi:10.5194/acp-9-3505-2009, 2009. 7799

Kullmann, A., M. Riese, F. Olschewski, F. Stroh, K.-U. Grossmann: Cryogenic Infrared Spectrometers and Telescopes for the Atmosphere - New Frontiers, Proc. SPIE, 5570, 423–432, 2004. 7797

Kunz, A., Konopka, P., Müller, R., Pan, L. L., Schiller, C., and Rohrer, F.: High static stability in the mixing layer above the extratropical tropopause, J. Geophys. Res., 114, D16305, doi:10.1029/2009JD011840, 2009. 7810

ACPD
12, 7793–7827, 2012

McKenna, D. S., Konopka, P., Grooß, J.-U., Günther, G., Müller, R., Spang, R., Offermann, D., and Orsolini, Y.: A new Chemical Lagrangian Model of the Stratosphere (CLaMS) 1. Formulation of advection and mixing, J. Geophys. Res., 107, 4309, doi:10.1029/2000JD000114, 2002. 7796, 7799

McKenna, D. S., Grooß, J.-U., Günther, G., Konopka, P., Müller, R., Carver, G., and Sasano, Y.: A new Chemical Lagrangian Model of the Stratosphere (CLaMS) 2. Formulation of chemistry scheme and initialization, J. Geophys. Res., 107, 4256, doi:10.1029/2000JD000113, 2002. 7796, 7799

Offermann, D., Grossmann, K.-U., Barthol, P., Knieling, P., Riese, M., and Trant, R.: Crypgenic Infrared Spectrometers and Telescopes for the Atmosphere (CRISTA) erxperiment and middle atmosphere variability, J. Geophys. Res., 104, 16311–16325, 1999. 7796

Olsen, M. A., Douglass, A. R., Newman, P. A., Gille, J. C., Nardi, B., Yudin, V. A., Kinnison, D. E., and Khosravi, R.: HIRDLS observations and simulation of a lower stratospheric intrusion of tropical air to high latitudes, Geophys. Res. Lett., 35, L21813, doi:10.1029/2008GL035514, 2008. 7795

Pan, L. L., Randel, W. J., Gary, B. L., Mahoney, M. J., and Hintsa, E. J.: Definitions and sharpness of the extratropical tropopause: A trace gas perspective, J. Geophys. Res., 109, D23103, doi:10.1029/2004JD004982, 2004. 7795, 7807, 7810

Pan, L. L., Bowman,K. P., Shapiro, M., Randel, W. J., Gao, R. S., Campos, T., Davis, C., Schauffler, S., Ridley, B. A., Wei, J. C., and Barnet, C.: Chemical behavior of the tropopause observed during the Stratosphere-Troposphere Analyses of Regional Transport experiment, J. Geophys. Res., 12, D18110, doi:10.1029/2007JD008645, 2007. 7795, 7808

Park, M., Randel, W. J., Emmons, L. K., Bernath, P. F., Walker, K. A., and Boone, C. D.: Chemical isolation in the Asian monsoon anticyclone observed in Atmospheric Chemistry Experiment (ACE-FTS) data, Atmos. Chem. Phys., 8, 757–764, doi:10.5194/acp-8-757-2008, 2008. 7807

Purser, R.J. and Huang, H.L.: Estimating effective data density in a satellite retrieval or and objective analysis, J. Appl. Meteorol., 32, 1092–1107, 1993. 7801

Redelsperger, J.-L., Thorncroft, C. D., Diedhiou, A., Lebel, T., Parker, D. J., and Polcher, J.: African Monsoon Multidisciplinary Analysis, B. Am. Meteor. Soc., 87, 1739–1746, doi:10.5194/acp-9-3505-2009, 2006. 7795

Remedios, J. J., Leigh, R. J., Waterfall, A. M., Moore, D. P., Sembhi, H., Parkes, I., Greenhough, J., Chipperfield, M., and Hauglustaine, D.: MIPAS reference atmospheres and comparisons

ACPD
12, 7793–7827, 2012

to V4.61/V4.62MIPAS level 2 geophysical data sets, Atmos. Chem. Phys. Discuss., 7, 9973–10017, doi:10.5194/acpd-7-9973-2007, 2007. 7798
Riese, M., Tie, X., Brasseur, G., and Offermann, D.: Three-dimensional simulation of stratospheric trace gas distributions measured by CRISTA, J. Geophys. Res., 104, 16419–16435, doi:10.1029/1999JD900178, 1999. 7796
Riese, M., Manney, G. L., Oberheide, J., Tie, X., Spang, R., and Kuell, V.: Stratospheric transport by planetary wave mixing as observed during CRISTA-2, J. Geophys. Res., 107, 8179, doi:10.1029/2001JD000629, 2002. 7797
Riese, M., F. Friedl-Vallon, R. Spang, P. Preusse, C. Schiller, L. Hoffmann, P. Konopka, H. Oelhaf, Th. von Clarmann, M. Hopfner: GLObal limb Radiance Imager for the Atmosphere (GLORIA): Scientific objectives, Adv. Space Res., 36, 989–995, 2005. 7812
Rodgers, C. D.: Inverse Methods for Atmospheric Sounding: Theory and Practice, World Scientific, 2000. 7798
Schiller, C., Krämer, M., Afchine, A., Spelten, N., and Sitnikov, N.: Ice water content of Arctic, midlatitude, and tropical cirrus, J. Geophys. Res., 113, D24208, doi:10.1029/2008JD010342, 2008. 7799
Schroeder, S. E., Kullmann, A., Preusse, P., Stroh, F., Weigel, K., Ern, M., Knieling, P., Olschewski, F., Spang, R., and Riese, M.: Radiance calibration of CRISTA-NF, Adv. Space Res., 43, 1910–1917, 2009. 7797
Seo, K.-H., and Bowman, K. P.: Lagrangian estimate of global stratosphere-troposphere mass exchange, J. Geophys. Res., 107, 4555, doi:10.1029/2002JD002441, 2002. 7795, 7811
Shapiro, M. A.: Turbulent mixing within tropopause folds as a mechanism for the exchange of chemical constituents between the stratosphere and troposphere, J. Atmos. Sci., 37, 994–1004, 1980. 7795, 7810, 7811
Spang, R., Hoffmann, L., Kullmann, A., Olschewski, F., Preusse, P., Knieling, P., Schroeder, S., Stroh, F., Weigel, K., Riese, M.: High resolution limb observations of clouds by the CRISTA-NF experiment during the SCOUT-O3 tropical aircraft campaign, Adv. Space Res., 42, 1765–1775, 2008. 7795, 7797, 7798
Stefanutti, L., L. Sokolov, S. Balestri, A. R. MacKenzie, and V. Khattatov: The M-55 Geophysica as a Platform for the Airborne Polar Experiment, J. Atmos. Ocean. Technol., 16, 1303–1312, doi:10.1175/1520-0426, 1999. 7795, 7797
Talukdar, R. K., Burkholder, J. B., Schmoltner, A.-M., Roberts, J. M., Wilson, R. R., and Ravishankara, A. R.: Investigation of the loss processes for peroxyacetyl nitrate in the at-

ACPD
12, 7793–7827, 2012

mosphere: UV photolysis and reaction with OH, J. Geophys. Res., 100, 14163–14173, doi:10.1029/95JD00545, 1995. 7805

Ungermann, J., Hoffmann, L., Preusse, P., Kaufmann, M., and Riese, M.: Tomographic retrieval approach for mesoscale gravity wave observations by the PREMIER Infrared Limb-Sounder, Atmos. Meas. Tech., 3, 339–354, doi:10.5194/amt-3-339-2010, 2010. 7812

Ungermann, J., Blank, J., Lotz, J., Leppkes, K., Hoffmann, L., Guggenmoser, T., Kaufmann, M., Preusse, P., Naumann, U., and Riese, M.: A 3-D tomographic retrieval approach with advection compensation for the air-borne limb-imager GLORIA, Atmos. Meas. Tech., 4, 2509–2529, doi:10.5194/amt-4-2509-2011, 2011. 7812

Ungermann, J., Kalicinsky, C., Olschewski, F., Knieling, P., Hoffmann, L., Blank, J., Woiwode, W., Oelhaf, H., Hösen, E., Volk, C. M., Ulanovsky, A., Ravegnani, F., Weigel, K., Stroh, F., and Riese, M.: CRISTA-NF measurements with unprecedented vertical resolution during the RECONCILE aircraft campaign, Atmos. Meas. Tech. Discuss., 4, 6915–6967, doi:10.5194/amtd-4-6915-2011, 2011. 7797, 7801

Vogel, B., Konopka, P., Grooß, J.-U., Müller, R., Funke, B., Lopez-Puertas, M., Reddmann, T., Stiller, G., von Clarmann, T., and Riese, M.: Model simulations of stratospheric ozone loss caused by enhanced mesospheric NOx during Arctic Winter 2003/2004, Atmos. Chem. Phys., 8, 5279–5293, doi:10.5194/acp-8-5279-2008, 2008. 7796

von Clarmann, T.: Validation of remotely sensed profiles of atmospheric state variables: strategies and terminology, Atmos. Chem. Phys., 6, 4311–4323, doi:10.5194/acp-6-4311-2006, 2006. 7799

Waters, J., Froidevaux, L., Harwood, R. S., Jarnot, R. F., Pickett, H. M., Read, W. G., Siegel, P. H., Cofield, R. E., Filipiak, M. J., Flower, D. A., Holden, J. R., Lau, G. K., Livesey, N. J., Manney, G. L., Pumphrey, H. C., Santee, M. L., Wu, D. L., Cuddy, D. T., Lay, R. R., Loo, M. S., Perun, V. S., Schwartz, M. J., Stek, P. C., Thurstans, R. P., Boyles, M. A., Chandra, K. M., Chavez, M. C., Chen, G. S., Chudasama, B. V., Dodge, R., Fuller, R. A., Girard, M. A., Jiang, J. H., Jiang, Y. B., Knosp, B. W., LaBelle, R. C., Lam, J. C., Lee, K. A., Miller, D., Oswald, J. E., Patel, N. C., Pukala, D. M., Quintero, O., Scaff, D. M., Van Snyder, W., Tope, M. C., Wagner, P. A., and Walch, M. J., The Earth Observing System Microwave Limb Sounder (EOS MLS) on the Aura satellite, IEEE Trans. Geosci. Remote Sens., 44, 1075–1092, 2006. 7797

Weigel, K., Riese, M., Hoffmann, L., Hoefer, S., Kalicinsky, C., Knieling, P., Olschewski, F., Preusse, P., Spang, R., Stroh, F., and Volk, C. M.: CRISTA-NF measurements during the

ACPD
12, 7793–7827, 2012

AMMA-SCOUT-O3 aircraft campaign, Atmos. Meas. Tech., 3, 1437–1455, doi:10.5194/amt-3-1437-2010, 2010. 7795, 7797, 7798, 7799, 7801, 7802, 7811

Werner, A., Volk, C. M., Ivanova, E. V., Wetter, T., Schiller, C., Schlager, H., and Konopka, P.: Quantifying transport into the Arctic lowermost stratosphere, Atmos. Chem. Phys., 10, 11623–11639, doi:10.5194/acp-10-11623-2010, 2010. 7798

WMO: Scientific assessment of ozone depletion: 2006, Report No. 50, 572 Geneva, Switzerland, 2007. 7811

ACPD

12, 7793–7827, 2012

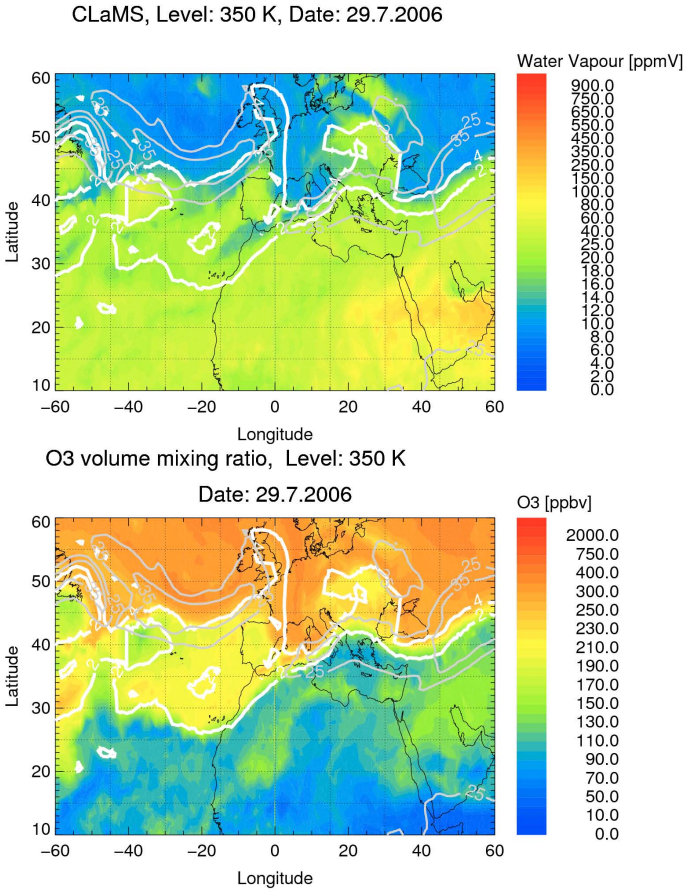

Fig. 1. Map of CLaMS H_2O and O_3 on the $\zeta = 350\,K$ level with 2 and 4 PVU line (white, solid) and horizontal wind speed of 25 and 35 $m\,s^{-1}$ from ECMWF (grey, solid) marking the position of the subtropical jet.

ACPD
12, 7793–7827, 2012

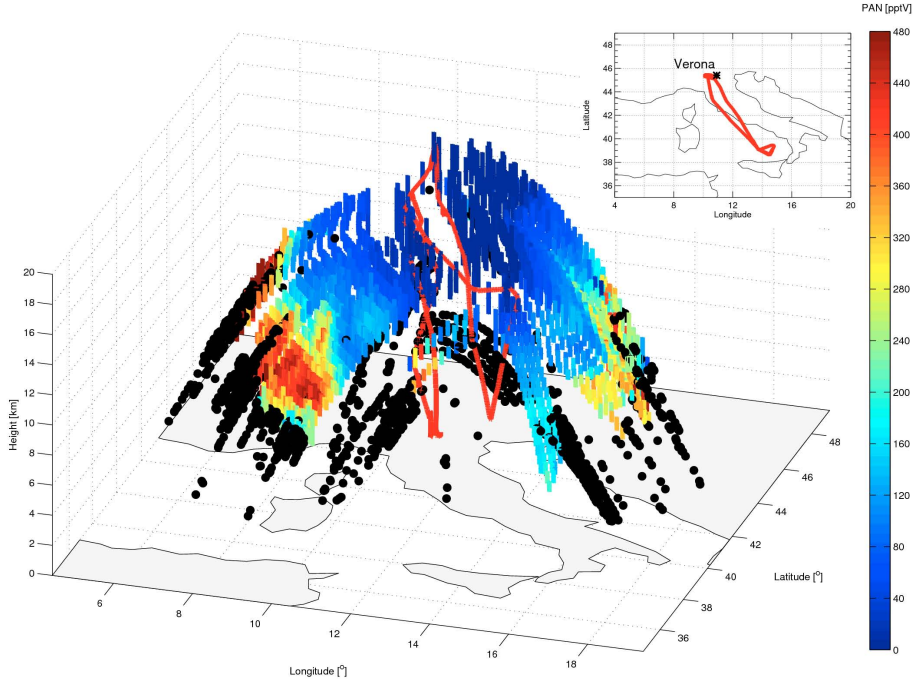

Fig. 2. Flight track and PAN mixing ratios as retrieved for the AMMA flight on 29 July 2006. Red line: Flight path, black dots: Cloud Index <3.5.

ACPD
12, 7793–7827, 2012

A stratospheric intrusion at the subtropical jet

K. Weigel et al.

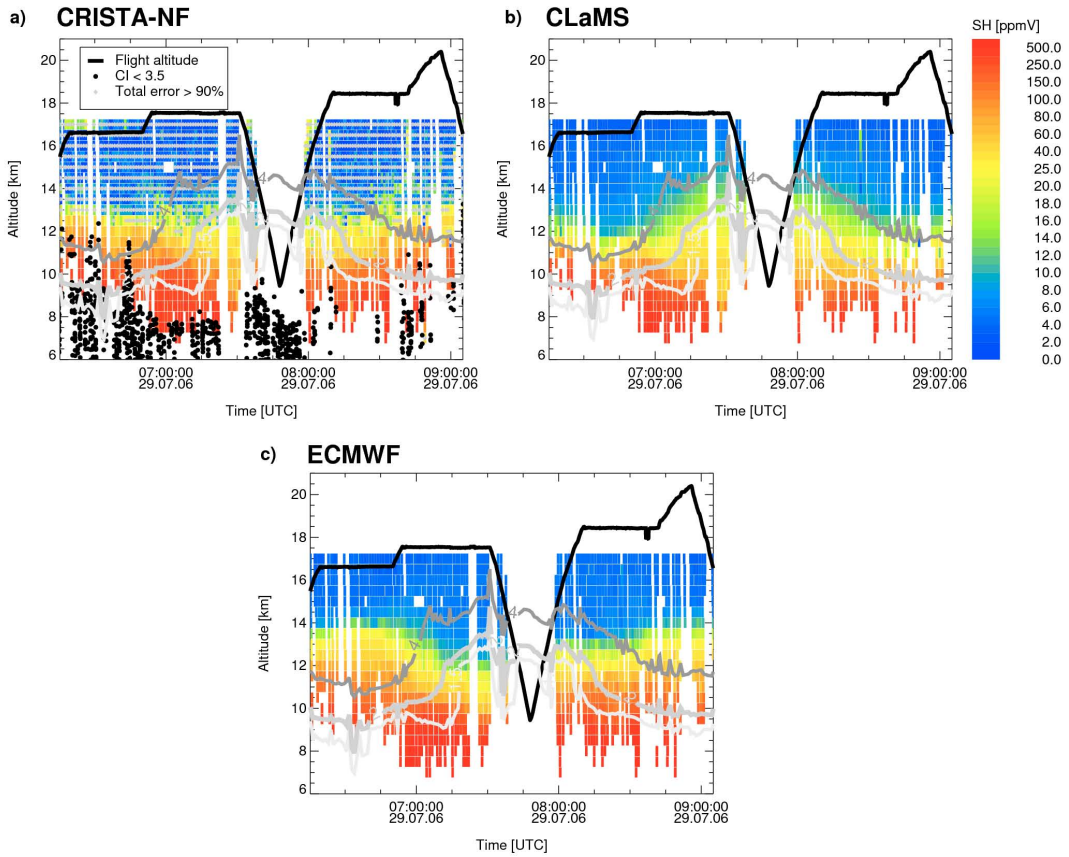

Fig. 3. H_2O from CRISTA-NF, CLaMS, and ECMWF analysis data. Colour scale shows the H_2O volume mixing ratio, gray lines show the ECMWF potential vorticity at 1.5, 2 and 4 PVU, black line the flight track, black dots spectra with optical dense conditions, grey diamonds retrieval results with a total error larger than 90 % (with CRISTA-NF H_2O). Note nonlinear colour scale.

ACPD
12, 7793–7827, 2012

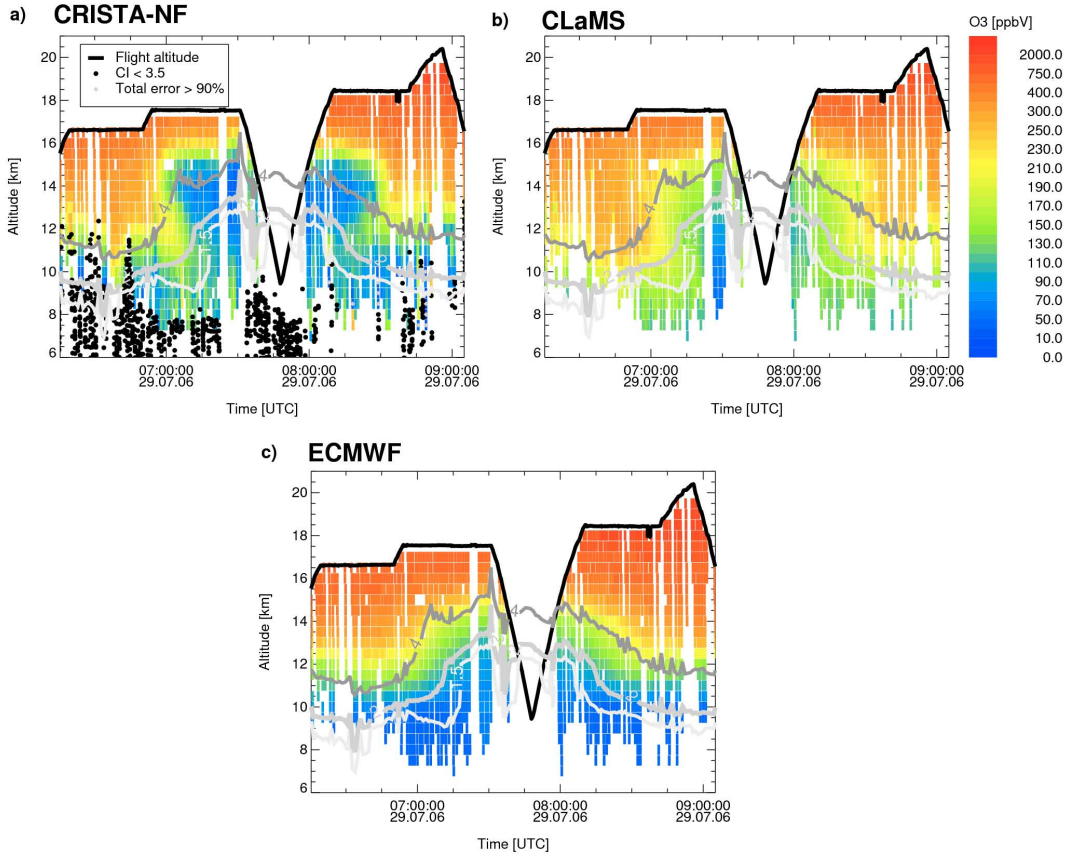

Fig. 4. O_3 from CRISTA-NF, CLaMS, and ECMWF analysis data. Colour scale shows the O_3 volume mixing ratio, gray lines show the ECMWF potential vorticity at 1.5, 2 and 4 PVU, black line the flight track, black dots spectra with optical dense conditions, grey diamonds retrieval results with a total error larger than 90 % (with CRISTA-NF O_3). Note nonlinear colour scale.

ACPD
12, 7793–7827, 2012

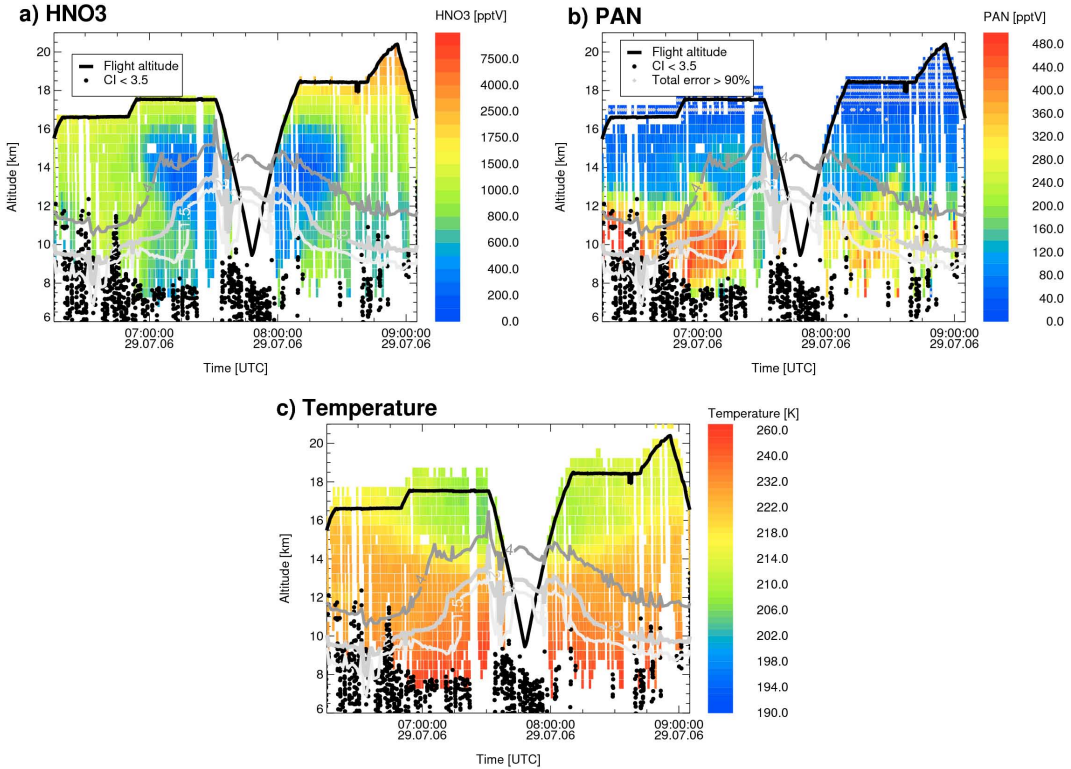

Fig. 5. CRISTA-NF retrieval results for HNO_3, PAN, and Temperature. Gray lines show the ECMWF potential vorticity at 1.5, 2 and 4 PVU, black line the flight track, black dots spectra with optical dense conditions, and grey diamonds retrieval results with a total error larger than 90 %. Note nonlinear colour scales.

ACPD
12, 7793–7827, 2012

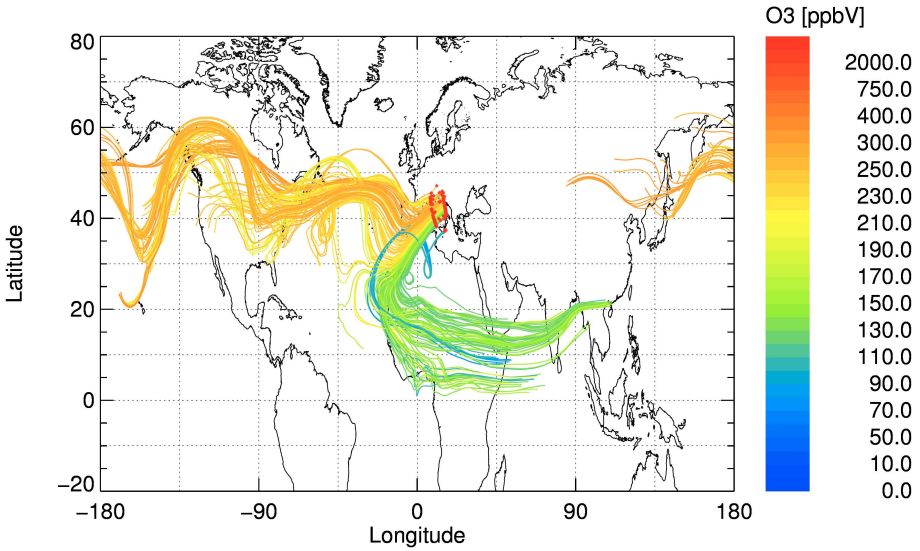

Fig. 6. Map with 10 day backward trajectories from the CRISTA-NF grid positions between 350 and 360 K ζ. Color coding shows the CLaMS O_3 on the CRISTA-NF grid (without filtering) during the flight on 29 July 2006. The measurement positions are marked with red diamonds.

ACPD
12, 7793–7827, 2012

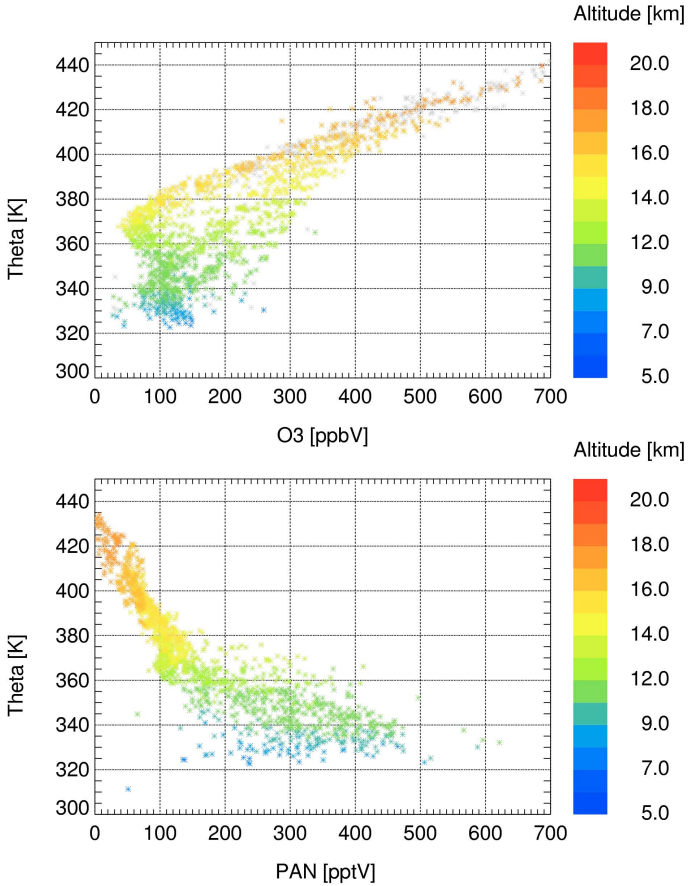

Fig. 7. Scatter plot of CRISTA-NF O_3 **(a)** and PAN **(b)** agains potential temperature. Color scales display the altitude of the measured mixing ratios, grey stars show values, with a vertical resolution coarser then 3 km.

ACPD
12, 7793–7827, 2012

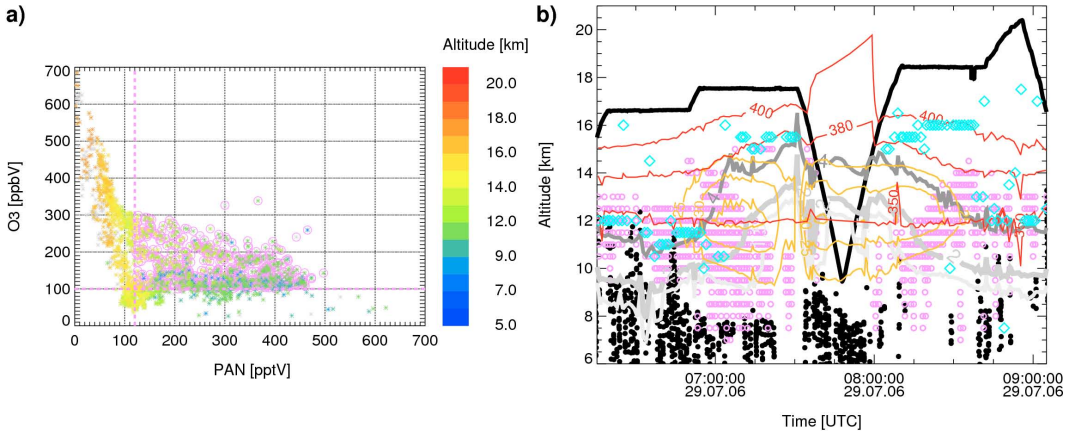

Fig. 8. Panel **(a)**: Scatter plot of CRISTA-NF O_3 and PAN. Color scales display the altitude of the measured mixing ratios. Pink circles indicate mixing identified through O_3 mixing ratios above 100 ppbV at the same time as PAN mixing ratios above 120 pptV. Panel **(b)**: Gray lines show the ECMWF potential vorticity at 1.5, 2 and 4 PVU, black line the flight track, and black dots the cloudy spectra. Red contour show ζ-level from CLaMS, light blue diamonds show the lapsrate tropopause from CRISTA-NF measurements, and gold contours show the horizontal ECMWF wind speed. Pink circles show positions, where the tracer-tracer correlation in Panel a indicates mixing.

ACPD
12, 7793–7827, 2012